Numerical investigation of droplet deformation in contraction nozzles containing shear-thinning fluids

A. Baniabedalruhman
Department of Mathematics, Yarmouk University, Irbid, Jordan
E-mail: *ahmad_a@yu.edu.jo*

Received 5 August 2026; accepted 30 September 2026; published online 2 November 2026
DOI https://doi.org/10.21595/vp.2026.27061

79th International Conference on Vibroengineering in Kaunas Lithuania, October 15, 2026

Copyright © 2026 A. Baniabedalruhman. This is an open access article distributed under the Creative Commons Attribution License, which permits unrestricted use, distribution, and reproduction in any medium, provided the original work is properly cited.

Abstract. A droplet entering a contraction does not see the same flow conditions throughout its passage. Here, numerical calculations are used to follow this deformation and determine when breakup occurs for three continuous liquids: one Newtonian and two shear-thinning fluids. The incompressible two-phase problem is solved in OpenFOAM with a Volume-of-Fluid formulation and a modified interDyMFoam solver, while local mesh refinement follows the interface. The droplet is Newtonian. The other two liquids are represented by the Bird–Carreau model and have different high-shear viscosities. For each selected streamline, the initial radius is varied until the limiting size between an intact and a broken droplet is located; the corresponding critical capillary number is then evaluated. The calculations show that elongation is strong but short-lived near the contraction, whereas shear persists farther downstream. They also show why shear rate alone can be misleading for a shear-thinning liquid: close to the wall the shear rate may increase while the viscous stress decreases because apparent viscosity has fallen. Two breakup forms are obtained, namely filament fracture and tip streaming with satellite droplets. The critical radius decreases sharply from the inner trajectories toward the wall and changes little thereafter. The three liquids remain separated when the breakup data are compared using shear rate, but this separation is greatly reduced with a scaled downstream shear-stress coordinate. For the cases considered, the breakup limit therefore reflects the combined changes in deformation rate, apparent viscosity, viscous stress, and viscosity ratio.

Keywords: droplet breakup, contraction nozzle, shear-thinning fluid, Bird-Carreau model, volume of fluid, adaptive mesh refinement.

1. Introduction

Emulsions, including double emulsions, are widely used to encapsulate or stabilize active ingredients in food, cosmetic, and pharmaceutical formulations [1]; [2]. Their behavior during processing is important as well. In spray drying, for example, atomization takes place before the solvent is removed, so changes to the droplets inside the nozzle can influence the particles produced afterward [3]; [4]. A contraction is particularly relevant because a droplet passing through it encounters changing shear and elongational fields rather than a uniform load. Breakup becomes possible when this loading overcomes the restoring effect of interfacial tension.

The capillary number provides the usual measure of this competition in Newtonian systems, as established in the classical studies of Taylor [6] and Grace [7]. With a shear-thinning continuous phase, however, the interpretation is less straightforward. As the deformation rate rises, the apparent viscosity falls. Consequently, a large shear rate does not necessarily correspond to a proportionally large viscous stress, and the viscosity ratio changes along the droplet path. Recent studies have examined related non-Newtonian effects during droplet formation in flow-focusing and cross-junction microchannels [8]; [9] and during droplet motion or breakup in other confined geometries [10]; [11].

The present calculations address breakup during passage through a contraction nozzle. Following the geometry and dynamic-mesh approach of earlier nozzle and interface-tracking work

 ISSN PRINT 2345-0533, ISSN ONLINE 2538-8479

[5]; [12], the same framework compares one Newtonian and two Bird–Carreau continuous liquids. The main novelty is the direct comparison of breakup limits under these rheologies and the use of downstream shear stress, rather than shear rate alone, as a common representation of breakup behavior. Along representative streamlines, we examine the loading history, breakup mode, limiting initial radius, and critical capillary number.

2. Mathematical and numerical model

A single droplet is followed through an axisymmetric contraction. Both phases are incompressible. The dispersed phase is Newtonian, while the continuous phase is assigned either constant viscosity or a Bird-Carreau shear-dependent viscosity. A Volume-of-Fluid (VOF) variable ϕ identifies the phases and tracks the moving interface. The governing equations are:

$$\nabla \cdot \mathbf{u} = 0, \tag{1}$$

$$\frac{\partial(\rho \mathbf{u})}{\partial t} + \nabla \cdot (\rho \mathbf{u}\mathbf{u}) = -\nabla p + \nabla \cdot (\eta \dot{\boldsymbol{\gamma}}) + \mathbf{F}_\sigma + \rho \mathbf{g}, \tag{2}$$

$$\frac{\partial \phi}{\partial t} + \nabla \cdot (\mathbf{u}\phi) = 0. \tag{3}$$

The continuum-surface-force representation is used for surface tension, $\mathbf{F}_\sigma = \sigma \kappa \nabla \phi$, with $\kappa = -\nabla \cdot (\nabla \phi / |\nabla \phi|)$. The rate-of-strain tensor is $\dot{\boldsymbol{\gamma}} = \nabla \mathbf{u} + (\nabla \mathbf{u})^T$. Mixture density and viscosity are interpolated through the VOF field.

2.1. Constitutive relation

The non-Newtonian continuous phases follow the Bird-Carreau model:

$$\eta(\dot{\gamma}) = \eta_\infty + (\eta_0 - \eta_\infty)[1 + (\tau \dot{\gamma})^2]^{(n-1)/2}. \tag{4}$$

where η_0 and η_∞ are the zero- and infinite-shear viscosities, τ is a characteristic time, and n is the flow-behavior index. The two non-Newtonian cases share η_0, τ, and n but have different η_∞, producing different reductions of apparent viscosity.

2.2. Geometry, fluid properties and boundary conditions

The computational geometry represents the converging part of a spraying nozzle. The upstream radius is $R_u = 3$ mm and the downstream radius is $R_d = 0.5$ mm, giving $R_u/R_d = 6$. The downstream channel is extended to 20 mm so that a strongly deformed droplet can evolve away from the outlet while breakup is assessed.

Table 1. Physical properties of the dispersed and continuous phases.

Fluid	Density (kg m^{-3})	η_0 (Pa s)	η_∞ (Pa s)	Model
Dispersed	918	0.0634	–	Newtonian
Continuous I	977	0.113	0.113	Newtonian
Continuous II	977	0.113	0.080	Shear-thinning
Continuous III	977	0.113	0.010	Strongly shear-thinning

For both non-Newtonian fluids, $\tau = 0.0049$ s and $n = 0.01323$, while the interfacial tension is $\sigma = 5.75 \times 10^{-3}$ N/m. A fully developed inlet profile is prescribed with average velocity $U = 0.0295$ m/s; no-slip and impermeability conditions are imposed at the wall, the centerline is a symmetry boundary, and the outlet uses a velocity zero-gradient condition with a fixed reference pressure.

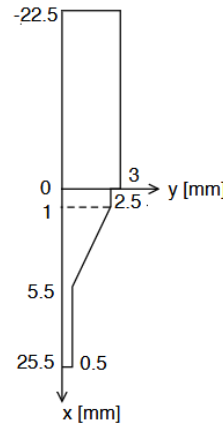


Fig. 1. Axisymmetric contraction geometry used in the simulations

2.3. Discretization, adaptive refinement and dimensionless parameters

The equations are discretized by the finite-volume formulation implemented in OpenFOAM. A modified interDyMFoam solver permits repeated refinement and unrefinement as the droplet travels through the nozzle. Refinement is concentrated around cells crossed by the interface, especially near breakup where thin necks and highly curved regions develop.

Mesh sensitivity was assessed using successively refined meshes by comparing velocity, pressure, interface evolution, and breakup response. The retained base mesh contains approximately 15 000 control volumes. Local cell sizes in the contraction and downstream region satisfy 0.02 mm $\leq h \leq$ 0.09 mm, with additional dynamic refinement restricted to the interface neighborhood.

The principal dimensionless groups are:

$$Re = \frac{\rho_c U D}{\eta_c}, \qquad \lambda = \frac{\eta_d}{\eta_c}, \qquad Ca = \frac{\eta_c \dot{\gamma} r_d}{\sigma}, \tag{5}$$

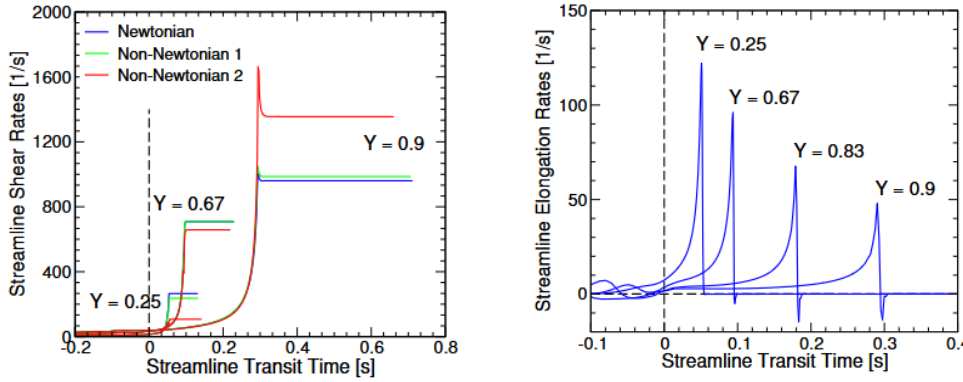
where $D = 2R_d$. For shear-thinning fluids, η_c is the local Bird-Carreau apparent viscosity. The inlet condition gives $Re = 0.764$ and $\lambda = 0.561$ for the Newtonian case; the corresponding ranges are $Re =$ 0.764-1.08 and $\lambda =$ 0.561-0.793 for continuous phase II, and $Re =$ 0.764-8.64 and $\lambda =$ 0.561-6.34 for continuous phase III.

3. Results and discussion

3.1. Single-phase loading field

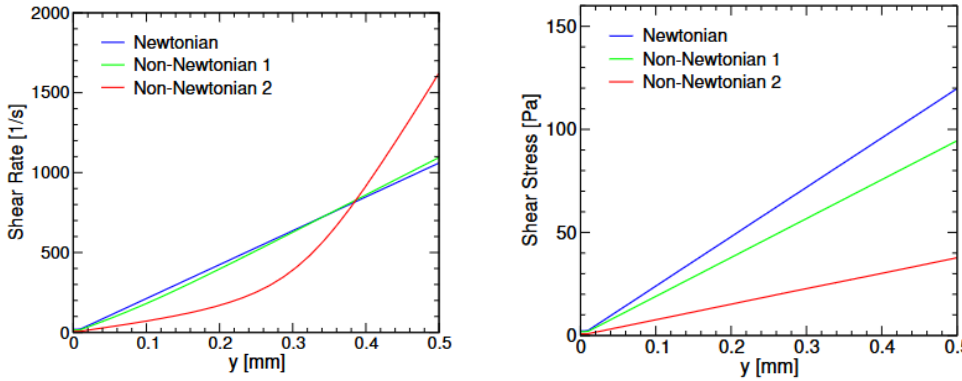
Before introducing a droplet, a steady single-phase solution is computed for each continuous phase. This separates the rheological effect from the disturbance produced by the droplet and provides the deformation-rate and stress histories subsequently experienced along the selected trajectories.

The shear rate increases sharply as the fluid accelerates through the contraction and remains important downstream. The elongational component has a more localized history: pronounced peaks occur as a streamline enters the contraction, after which the elongation rate falls toward zero. Thus, the droplet experiences strong elongation mainly during entry into the contraction, whereas shear supplies a longer-lasting downstream load. Rheology redistributes the deformation rate; the strongly shear-thinning fluid can exhibit a steep near-wall increase in shear rate even though its apparent viscosity is substantially reduced.



a) Shear rate b) Elongation rate

Fig. 2. Representative loading histories along selected streamlines



a) Shear rate b) Shear stress

Fig. 3. Fully developed downstream profiles for the three continuous phases

The downstream profiles emphasize the distinction. Shear rate rises from the axis toward the wall for all three liquids and is steepest for the strongest shear-thinning case. The stress ordering is reversed: the Newtonian liquid carries the largest shear stress and the strongly shear-thinning liquid the smallest. Hence a near-wall droplet can encounter a high shear rate without experiencing the highest viscous stress.

3.2. Droplet tracking and breakup mechanisms

Droplets are released on selected streamlines in the fully developed upstream section. Their initial transverse positions are represented by $Y = y/R_u$. For each streamline and continuous phase, the initial radius is varied in successive simulations until the transition between stable deformation and breakup is bracketed. The reported critical radius is estimated from the largest tested radius that remains intact and the neighboring radius that fragments.

The dynamic mesh remains active throughout this search. As the droplet elongates, the finest cells follow the interface while the remainder of the domain stays comparatively coarse. This is particularly important close to breakup, when thin necks and strongly curved regions appear.

Two distinct breakup sequences are obtained. In filament fracture, the droplet stretches into a long filament, several necks form, and continued thinning divides the filament into daughter droplets. This occurs at the lower end of the breakup capillary-number range considered. In the second mode, the central portion remains comparatively thick while a thin trailing region releases small satellite droplets. Within the axisymmetric model this behavior is referred to as tip streaming. Both modes are found for Newtonian and shear-thinning continuous phases, with tip

streaming appearing as the local capillary number increases.

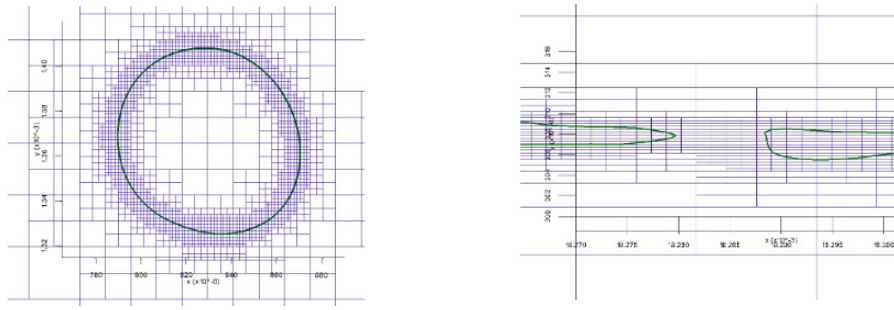
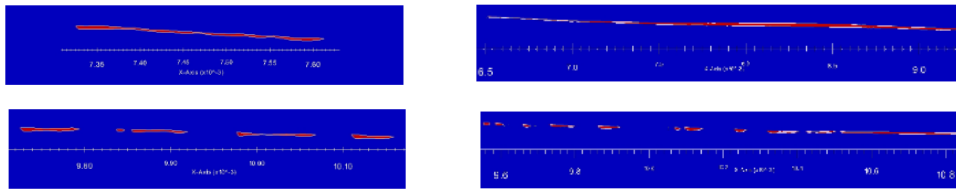


Fig. 4. Adaptive mesh refinement concentrated around the moving droplet interface

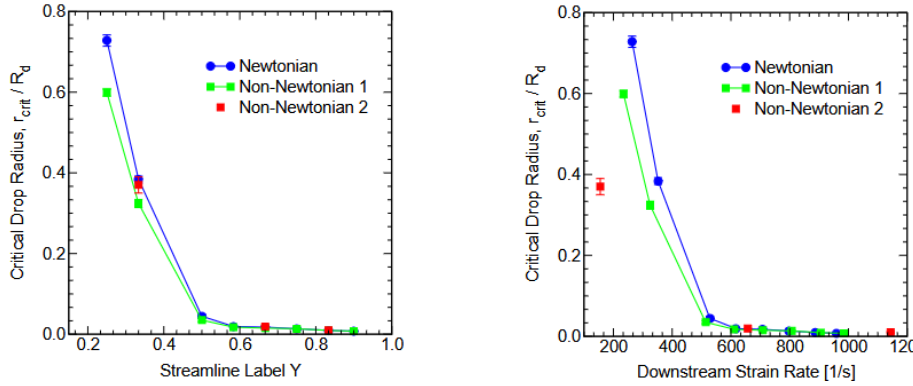


a) Filament fracture b) Tip streaming

Fig. 5. Two simulated droplet-breakup sequences

3.3. Critical droplet radius

The critical-radius calculations are repeated for each selected streamline and continuous phase. The resulting threshold is a numerically resolved stable/breaking bracket rather than an exact analytical critical value.



a) Versus streamline position Y b) Versus downstream shear rate

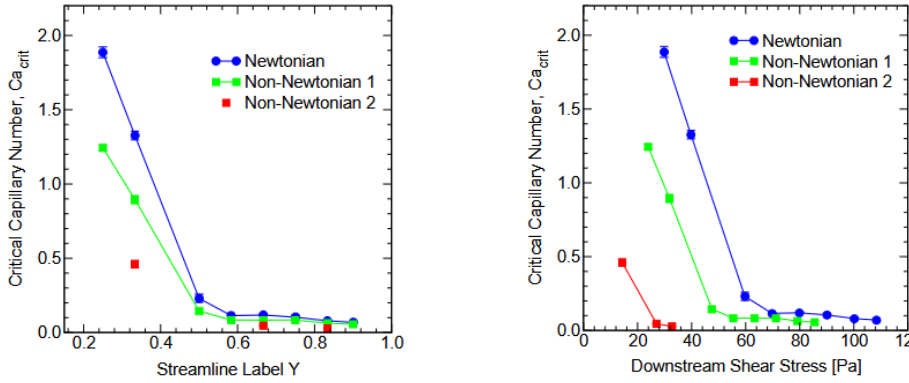
Fig. 6. Normalized critical droplet radius for Newtonian and non-Newtonian continuous phases

The strongest variation occurs between the inner and intermediate streamlines. As *Y* increases, the normalized critical radius falls sharply; farther toward the wall, the threshold approaches a small plateau. Plotting the same data against downstream shear rate gives a similar overall decrease, but the three fluids remain separated. This confirms that shear rate alone does not incorporate the rheology-induced reduction in apparent viscosity.

3.4. Critical capillary number and stress-based representation

For each critical-radius point, a critical capillary number is formed using the downstream

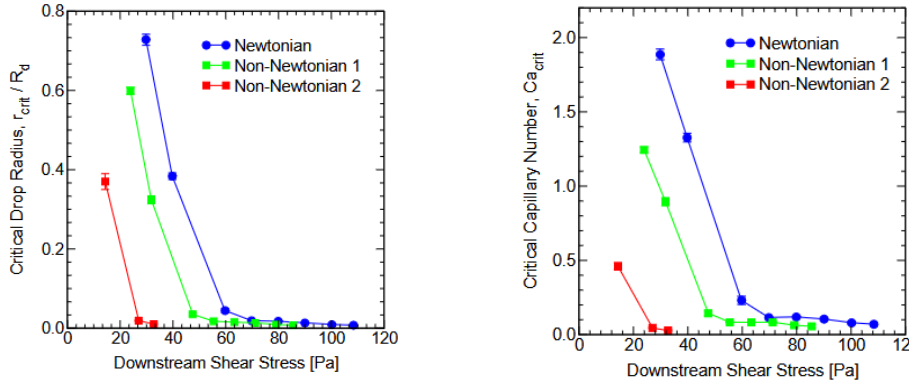
apparent viscosity and shear rate. It decreases markedly from the inner streamlines and changes much less as the wall is approached. The largest differences among rheologies occur where both the apparent viscosity and critical droplet size are changing rapidly.



a) Ca_{crit} versus Y b) Ca_{crit} versus shear stress

Fig. 7. Critical capillary number for the investigated trajectories

Because shear rate does not account for viscosity reduction, the breakup data are also represented against downstream shear stress. The critical radius decreases as stress increases, and the critical capillary numbers follow a similar progression for all three liquids. Compared with the shear-rate representation, the stress-based plots make the common behavior of the Newtonian and shear-thinning cases more apparent.



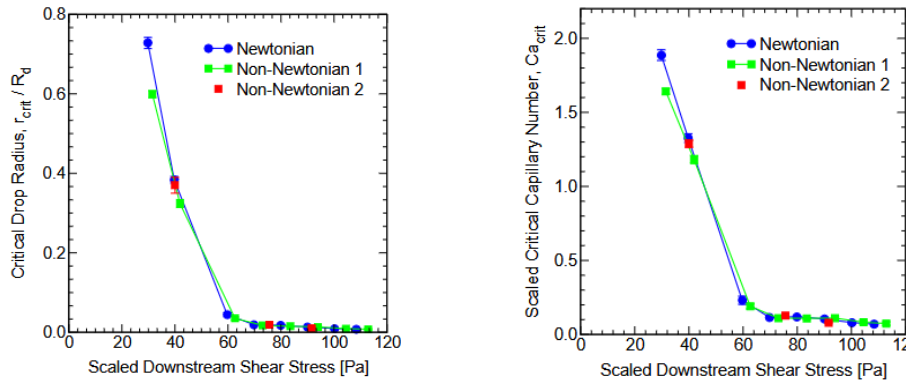
a) Critical radius b) Critical capillary number

Fig. 8. Breakup thresholds represented against downstream shear stress

A final comparison uses a scaled downstream shear-stress coordinate. The scaling is applied to the stress coordinate rather than to the observed breakup outcome, so the degree of collapse directly indicates whether this normalization is useful for comparing different continuous-phase rheologies.

After rescaling, the data lie close to common curves despite the substantial difference between the Newtonian viscosity and the high-shear viscosities of the Bird–Carreau liquids. Taken together, the results show that the breakup threshold is controlled by more than the local shear rate. Shear thinning changes apparent viscosity, viscous stress, and viscosity ratio simultaneously. This explains why the fluids remain separated in a shear-rate plot but approach a common trend when a scaled downstream-stress coordinate is used. The stress-based representation should not be interpreted as a universal breakup law; the present calculations concern one axisymmetric contraction, one dispersed-phase viscosity, fixed interfacial tension, and a limited set of

Bird-Carreau parameters.



a) Scaled critical radius b) Scaled critical capillary number

Fig. 9. Breakup characteristics represented by scaled downstream shear stress

4. Conclusions

Droplet deformation and breakup in a contraction nozzle were studied numerically for one Newtonian and two Bird-Carreau continuous phases. The simulations combined a VOF formulation with adaptive dynamic mesh refinement concentrated around the moving interface. The contraction creates a short region of strong elongation, while shear persists farther downstream. Shear thinning redistributes the shear rate, particularly near the wall, but the accompanying reduction in apparent viscosity lowers the viscous stress relative to the Newtonian case. Therefore, a high local shear rate does not necessarily correspond to the largest hydrodynamic loading.

Two breakup sequences were observed: filament fracture and a tip-streaming mode involving satellite droplets. Filament fracture occurred at the lower end of the breakup capillary-number range considered, whereas tip streaming appeared as the capillary number increased. The limiting droplet radius depended strongly on trajectory, decreasing from the inner region toward the wall before approaching a near-wall plateau. A similar trend was obtained for the critical capillary number.

The effect of shear thinning was not monotonic when described only by shear rate or viscosity. The breakup limit reflects simultaneous changes in apparent viscosity, viscous stress, and viscosity ratio. Expressing the critical-radius and critical-capillary-number data using a scaled downstream shear-stress coordinate brought the Newtonian and shear-thinning cases close to common curves. For the nozzle and material parameters investigated, stress-based scaling therefore provides the more consistent comparison of breakup conditions. Future work should examine fully three-dimensional breakup, broader rheological parameter ranges, and additional nozzle geometries.

Acknowledgements

The author has not disclosed any funding.

Data availability

The datasets generated during and/or analyzed during the current study are available from the corresponding author on reasonable request.

Conflict of interest

The author declares no conflict of interest.

References

[1] F. Leal-Calderon, J. Bibette, and V. Schmitt, *Emulsion Science: Basic Principles*. New York, NY: Springer New York, 2007, https://doi.org/10.1007/978-0-387-39683-5

[2] K. Pays, J. Giermanska-Kahn, B. Pouligny, J. Bibette, and F. Leal-Calderon, "Double emulsions: how does release occur," *Journal of Controlled Release*, Vol. 79, No. 1-3, pp. 193–205, 2002, https://doi.org/10.1016/s0168-3659(01)00535-1

[3] A. Aserin, *Multiple Emulsions: Technology and Applications*. Hoboken, NJ, USA: Wiley, 2007, https://doi.org/10.1002/9780470209264

[4] B. N. Dubey and E. J. Windhab, "Iron encapsulated microstructured emulsion-particle formation by prilling process and its release kinetics," *Journal of Food Engineering*, Vol. 115, No. 2, pp. 198–206, 2013, https://doi.org/10.1016/j.jfoodeng.2012.10.013

[5] K. Feigl, A. Baniabedalruhman, F. X. Tanner, and E. J. Windhab, "Numerical simulations of the breakup of emulsion droplets inside a spraying nozzle," *Physics of Fluids*, Vol. 28, No. 12, Dec. 2016, https://doi.org/10.1063/1.4972097

[6] G. I. Taylor, "The formation of emulsions in definable fields of flow," *Proceedings of the Royal Society of London. Series A, Containing Papers of a Mathematical and Physical Character*, Vol. 146, No. 858, pp. 501–523, 1934, https://doi.org/10.1098/rspa.1934.0169

[7] H. P. Grace, "Dispersion phenomena in high viscosity immiscible fluid systems and application of static mixers as dispersion devices in such systems," *Chemical Engineering Communications*, Vol. 14, No. 3-6, pp. 225–277, 1982, https://doi.org/10.1080/00986448208911047

[8] H. Cao, Y. Lu, L. Wu, C. Zhang, and L.-L. Zhang, "Shear-thinning fluid droplets formation in axisymmetric flow-focusing microfluidics," *Industrial and Engineering Chemistry Research*, Vol. 63, No. 8, pp. 3766–3779, 2024, https://doi.org/10.1021/acs.iecr.3c03947

[9] M. Fatehifar, A. Revell, and M. Jabbari, "Non-Newtonian droplet generation in a cross-junction microfluidic channel," *Polymers*, Vol. 13, No. 12, p. 1915, Jun. 2021, https://doi.org/10.3390/polym13121915

[10] R. Kumar, R. Lakkaraju, and A. Atta, "Shear-thinning rheology and geometric asymmetry govern droplet dynamics in branched microchannels," *Soft Matter*, Vol. 22, No. 8, pp. 1797–1808, Feb. 2026, https://doi.org/10.1039/d5sm00957j

[11] D. J. Meer, S. Sista, M. D. Shattuck, C. S. O'Hern, and E. R. Weeks, "Droplet breakup against an isolated obstacle," *Soft Matter*, Vol. 22, No. 15, pp. 2809–2822, Apr. 2026, https://doi.org/10.1039/d5sm01266j

[12] A. Baniabedalruhman, "Dynamic meshing around fluid-fluid interfaces with applications to droplet tracking in contraction geometries," Michigan Technological University, Houghton, MI, USA, 2015, https://doi.org/10.37099/mtu.dc.etds/1005